Heliyon 10 (2024) e26703

Contents lists available at ScienceDirect

Heliyon

journal homepage: www.cell.com/heliyon

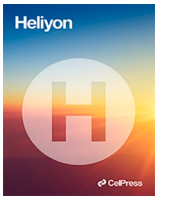

Research article

Effect in variation of the cationic precursor temperature on the electrical and crystalline properties of MnS growth by SILAR

H. Moreno-García [a], J.O. Sigala-Valdez [b], Ma del Rosario Martínez-Blanco [c], I. Cruz Reyes [d], S.M. Durón-Torres [b], I.L. Escalante-García [b], A. Del Rio-De Santiago [c,*]

[a] *Laboratorio Nacional-CIACyT, Universidad Autónoma de San Luis Potosí, Av. Sierra Leona # 550, Lomas 2a Sección, San Luis Potosí, SLP C.P. 78210, Mexico*

[b] *Unidad Académica de Ciencias Químicas, Universidad Autónoma de Zacatecas, Campus Universitario Siglo XXI, Carr. Zacatecas – Guadalajara Km. 6. Col. Ejido "La Escondida" Zacatecas, Zacatecas, C.P. 98160, Mexico*

[c] *Posgrado en ingeniería y tecnología aplicada, Unidad Académica de Ingeniería / Universidad Autónoma de Zacatecas., Ramón López Velarde 801, C.P. 98000, Zacatecas, Mexico*

[d] *Tecnológico Nacional de México. Instituto Tecnológico de Tijuana, Centro de Graduados e Investigación en Química, Blvd. Alberto Limón Padilla S/n, Col. Otay, Tecnológico, Tijuana, BC C.P. 22510, Mexico*

A R T I C L E I N F O

Keywords:
Manganese sulfide
SILAR
Thin film growth
Precursor temperature

A B S T R A C T

The crystallographic, optical, and electrical properties of manganese sulfide thin films depend on the control of the temperature precursors in the synthesis process, as shown by the results of this work. MnS thin films were deposited on glass substrates using the SILAR method and over an additional layer of CdS synthesized by chemical bath deposition (CBD) to acquire a p-n heterojunction. SILAR is an inexpensive method performed with a homemade robot in this case. Temperature in the solution precursors varied from 20 to 80 °C in four experiments. The morphology and structure of MnS and FTO/CdS/MnS thin films were studied through scanning electron microscopy (SEM) and grazing-incidence X-ray diffraction (GIXRD); the results indicate that materials showed a polycrystalline behavior, a diffraction peak of ***α***- MnS cubic phase was observed with lattice constants values, ranging from 4.74 to 4.75 Å.

Additionally, Raman spectroscopy showed a signal corresponding to the transversal optical phonons of MnS at a wavenumber near 300 cm^{-1}. UV–vis spectroscopy showed optical bandgap values of 3.94, 4.0, 4.09, and 4.26 eV for thin films obtained at 20°, 40°, 60°, and 80 °C.

respectively. Results indicated 80 °C as an optimal cationic precursor process temperature, achieving optical transmittance T% and good film quality according to SEM and GIXRD for the synthetization of MnS. The current–voltage (I–V) characterization in the heterojunction showed a characteristic diode curve with an open circuit voltage (VOC) of 300 mV under illumination, which indicated that the manganese sulfide behaves as p-type material contributing with positive charge carriers, while CdS behaves as n-type material.

* Corresponding author.
E-mail address: risa008537@uaz.edu.mx (A. Del Rio-De Santiago).

https://doi.org/10.1016/j.heliyon.2024.e26703
Received 20 September 2023; Received in revised form 16 February 2024; Accepted 19 February 2024
Available online 20 February 2024

1. Introduction

Materials presenting ferromagnetic behavior, like MnS, show properties related to two main branches of materials science: semiconductors and ferromagnetic materials [1–5] are of considerable current interest. These characteristics could promote the development of devices with both degrees of freedom, such as magnetic random-access memories, diodes and solar cells [1–3,6,7]. MnS is one example of the so-called diluted magnetic semiconductors (DMS), the subject of extensive research in the last few years [8, 9].

In recent years, the preparation of thin film semiconductors by SILAR has gained importance due its affordability, usability and the possibility of operating the process in extensive areas in contrast to other deposition techniques that commonly need ultra-high vacuum and very low temperatures [10]. Additionally, the SILAR slow-growth process, promotes a better orientation of crystallites and improves the grain structure [11].

The SILAR methodology for the deposit of films was developed in the mid-1980s independently by Ristov [12] and Nicolau et al. [13] to synthesize chalcogenides coatings (Fig. 1). This method involves a sequential immersion of the substrate in cationic and anionic solutions, the growth of the crystals is realizing ion-by-ion condensation and the adsorption of precursor's colloidal particles (cluster-by-cluster) onto a substrate. A modified SILAR process was develop consisting of changes in synthesis parameters, such as cationic precursor temperature, called pseudo-SILAR (p-SILAR) [14]. A notorious advantage of using p-SILAR, unlike other wet chemical or enhanced hydrothermal methods, is the reduction in time, the amount of chemical reagents, and the simplification of the chemical mechanisms involved in the process [15,16].

2. Methods

2.1. MnS thin films

In order to obtain the thin films of MnS, $MnCl_2$ 0.1 M and Na_2S 0.05 M were used as cationic and anionic precursor solutions. Glass slices were cleaned first in acetone, then in a 1:1 ethanol: water solution. The SILAR film deposit and growth required the four-step cycle process depicted in Fig. 1, that included the stages: 1) the substrate is immersing for 30s in the cationic solution to achieve the adsorption of the Mn^{2+} ions, 2) rinsing of substrate with DWI water for 50s to remove unabsorbed cationic species; 3) immersing the substrate in the anionic precursor by 30s to produce the S^{2-} ions reaction with the absorbed Mn^{2+} ions to form the MnS thin layer and finally, 4) rinsing the substrate again in DWI water for 50s to separate the unreacted anionic species loosely bound to the MnS particles.

The film thickness was estimated by using profilometry technique and correlated by transversal view of SEM images. Thin films thickness values for the CdS/MnS structure were: 204.2 ± 21.7, 112.6 ± 6.5, 176.4 ± 5.1, and 124.6 ± 18.0 nm, corresponding to deposition temperatures of: 25, 40, 60, and 80 °C respectively using standard error formula $\epsilon = \overline{x} \pm s$, where $\overline{x}$ is average thickness value and s is the statics standard deviation. Finally, the films were oven annealed at 300 °C for 1 h in a furnace [17].

The chemical reactions involved in the process were:

$$SnO_2 : F + MnCl^{-[solution]} \rightarrow SnO_2 : FMnCl^{[Absorbed]} + HCl \quad (1)$$

$$SnO_2 : FMnCl^{[Absorbed]} + NaS^{-[solution]} \rightarrow \vee MnS^{[Absorbed]} + NaOH \quad (2)$$

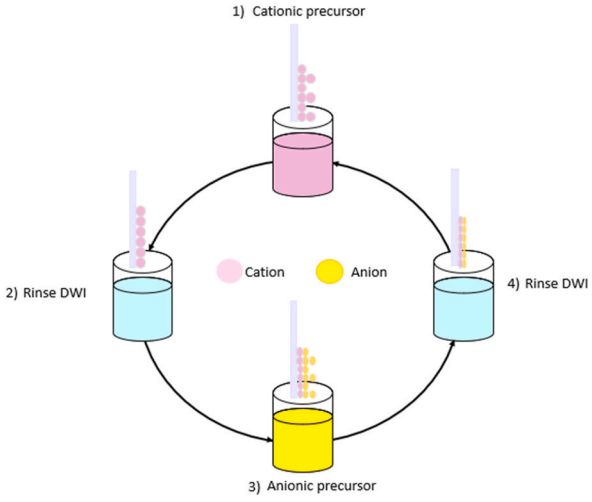

Fig. 1. Schematic diagram of the SILAR process: 1) Immersion to the cationic precursor, 2) First rinse in DWI, 3) Immersion to the anionic precursor, 4) Second rinse in DWI.

The cadmium sulfide (CdS) films were deposited on FTO glass substrates by chemical bath deposition technique. The following formulation was used by the successive addition: 25 ml 1 M of cadmium chloride, 15 ml 1 M of sodium citrate, 2 ml–3.7 M of ammonium hydroxide (aq.), 5 ml 1 M of thiourea and distiller water. A constant temperature bath was used at 80 °C during deposition for 1 h, according to Ref. [18]. Subsequently, the samples were removed from the solution and rinsed with plenty of distilled water for several seconds. It is important to remove excess dust on the film with a wet cotton pad. The thin films are considered to have a thickness of 100 nm with 1 h of deposition, according to Nair et al. reported.

2.1.1. Diode

For the elaboration of the multilayer structure, FTO glass substrates of 3 mm thickness with a commercial transparent conductive oxide (SnO_2: F) coating (SIGMA ALDRICH Fluorine doped tin oxide coated glass slide 50 mm × 3 mm) were used. At first, a CdS thin film is deposited by chemical bath deposition followed by a MnS thin film deposited by the SILAR method, while the temperature was varied in the range from room temperature to 80 °C at atmospheric pressure. During CdS thin films deposition, the adsorption and reaction times were evaluated from preliminary experiments, so that a layer deposition occurred and resulted in a homogeneous thin film structure. It is worth mentioning that six samples of MnS were made under identical conditions for the diode device with a final CdS layer to ensure reproducibility. Typical layered assemblies are shown in Fig. 2. Electrical contacts of Graphite paint (SPI-Chem) were placed on MnS thin was used for with an area of 0.5 cm^2.

2.2. Film characterization

For structural characterization, a PANalytical, grazing-incidence X-Ray Diffractometer with a Cu Ka radiation source ($\lambda = 1.5405$ Å) was used, the diffraction patterns of films were obtained by scanning the 2Θ angle in the range from 10| to 80°. The Horiba XploRA Plus microscope was employed to acquire the RAMAN spectra of the thin films. Measurements were made at room temperature using a 532 nm DPSS laser through a 100 × objective for an effective 1 mW applied power on the sample surface. The aforementioned spectra were acquired with an 1800 gr/mm grating and thermoelectrically cooled CCD for 10 s in 3 accumulations. The reflectance and transmittance UV–vis measurements were carried out by using a SHIMADZU V-3600 plus spectrometer with a wavelength resolution better than ±0.3 nm at room temperature. The electrical characterization of the diode samples was made using a Sciencetech solar simulator to measure electrical current-voltage curves. Thin films of manganese sulfide were first synthetized on a glass substrate, in order to determine the physical properties of the single MnS thin film; subsequently, a manganese sulfide film was deposited onto a CdS/FTO assembly to characterize the multilayer structure.

3. Results and discussion

3.1. XRD

Crystallographic properties of the (002) diffraction peak for all the diffractograms respectively were calculated using Debye Scherrer's equation $D(nm) = 0.9\lambda/\beta \cos\theta$ [19], where θ, β ,D and λ are Bragg's diffraction angle, FWHM, grain size, and X-Ray wavelength of all the samples evaluated by GIXRD patterns, this is shown in Table 1. Additionally, the dislocation density (δ) was calculated using $\delta(nm^{-2}) = 1/D^2$ [20] to have more information on the number of defects in the film. Finally, we use the Stokes- Wilson equation [20] to calculate the average strain values (ε_{str}). These results are in agreement with the literature [21,22] and could explain the quality of the thin film.

The XRD pattern (Fig. 3) is characteristic of the mix of tin oxide and cubic $\alpha-$ MnS; the lattice constant value was calculated using Bragg equation:

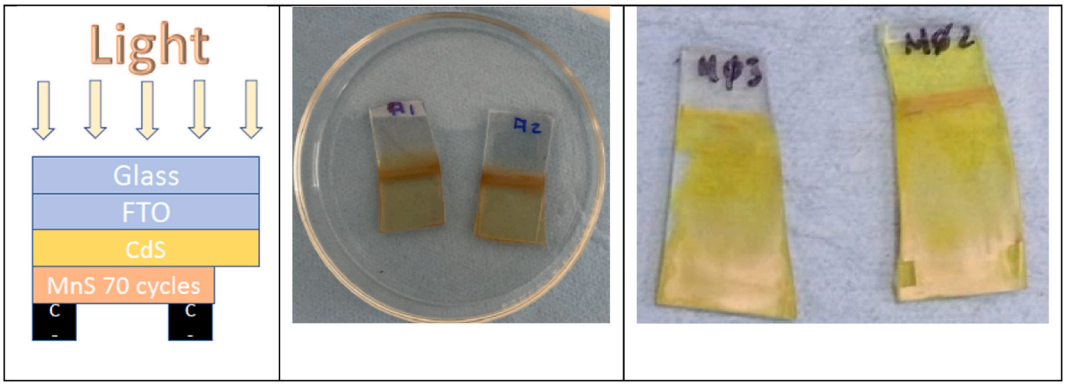

Fig. 2. Samples for the device with FTO/CdS/MnS, the device configuration is superstrate and the incident light strikes the glass surface with semitransparent contact.

Table 1
XRD Parameters and results for the thin films evaluated.

Compound	θ/°	β	D/nm	a/ Å	δ/nm^{-2}	ϵ_{str}/nm
MnS 20 °C	18.98	5.63×10^{-3}	26.04	4.73	1.47×10^{-3}	4.09×10^{-3}
MnS 40 °C	18.99	5.97×10^{-3}	24.56	4.74	1.66×10^{-3}	4.33×10^{-3}
MnS 60 °C	18.94	5.42×10^{-3}	27.04	4.74	1.37×10^{-3}	3.96×10^{-3}
MnS 80 °C	18.93	5.12×10^{-3}	28.63	4.75	1.22×10^{-3}	3.73×10^{-3}

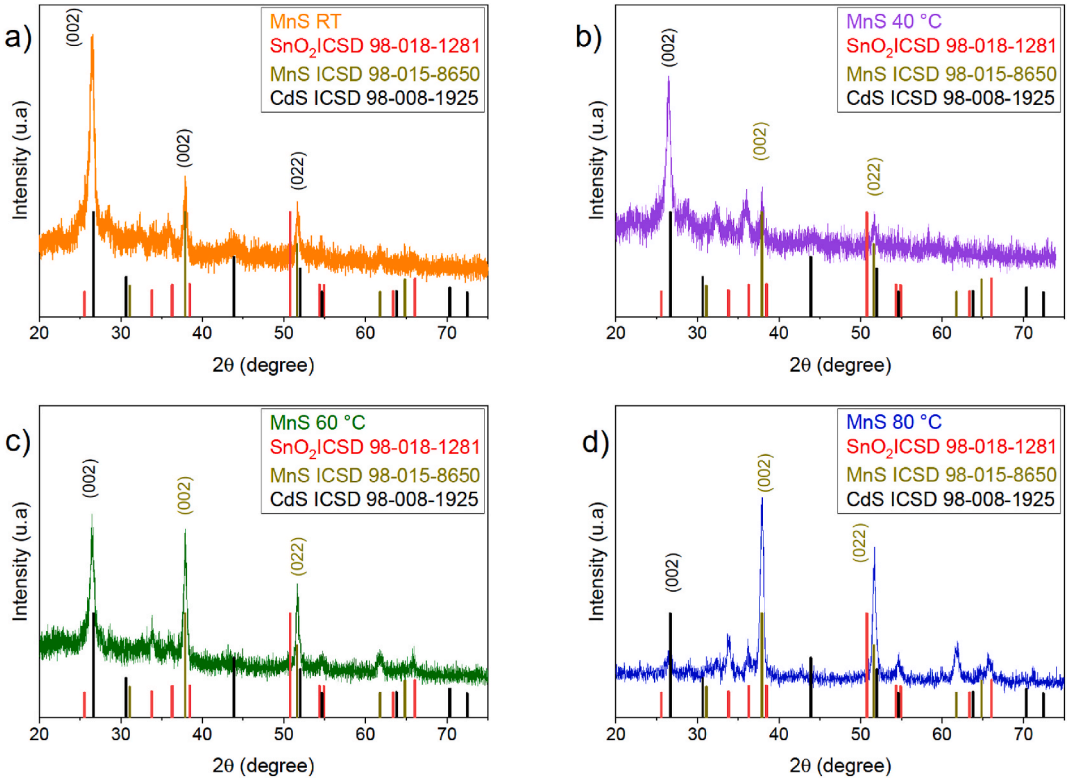

Fig. 3. Grazing-incidence X-ray diffraction pattern of MnS/CdS/FTO thin film deposited with a cationic precursor at a) room temperature, b) 40 °C, c) 60 °C and d) 80 °C and expected pattern for manganese sulfide, cadmium sulfide and for tin oxide.

$$n\lambda = 2dsin\theta \tag{3}$$

Where $\lambda = 0.154056nm, \theta = 51.68$ and d, are the X-Ray wavelength, diffraction angle of (002) diffraction peak, respectively, and lattice planes spacing, for a cubic structure constant can be calculated by:

$$\frac{1}{d^2_{(hkl)}} = \left(h^2 + k^2 + l^2\right)\frac{1}{a^2} \tag{4}$$

The grazing-incidence X-ray Diffraction (GIXRD) exhibited the polycrystalline nature of the α -MnS layer on FTO/CdS substrates. Fig. 3 shows the GIXRD patterns of MnS α-cubic type thin film deposited on FTO at different temperatures, we observed the preferential diffraction patterns for the tin oxide corresponding to the FTO [20] and this effect can be attributed to the ω angle used in the GIXRD. Even so, the appearance of the diffraction planes at 38.075 and 51.92 of 2θ. It can be cataloged as the preferential orientation signal for the (002) and (022) α-MnS according to the ICSD No. 98-015-8650 and analyzed by HighScore Plus software. Raman spectroscopy (Fig. 3) corroborates such data by observing the corresponding peak at 300 cm-1 TO signal associated with the MnS α-cubic type.

From Fig. 3 for the signal peak at 38.075 2 θ with a diffraction index of (002) we determined that is associated with cubic MnS. The effect in the precursor temperature has an observable effect on the height of the diffraction peaks, the temperature of 20 °C in the cationic precursor exhibit the least pronounced intensity for the MnS diffraction peak. As the temperature increases to 80 °C, we can observe that the manganese diffraction peak becomes thinner and more intense compared to those of the other components of the samples, that is, the manganese deposition improves with more temperature in the precursor, the decrease in FWHM indicates larger crystals and quality. The opposite effect is determined for the diffraction peak associated with CdS, which probably, is below the MnS in the sample, and is not reached by the configuration of the GIXRD. This is based on the behavior of the peaks associated with the

substrate.

3.2. Raman spectroscopy

Fig. 4 shown the Raman spectra of MnS/CdS/FTO. Peaks at 300 cm^{-1} correspond to the transversal optical phonon (TO) mode (A1/E1) [14], corresponding to the MnS layer. Raman spectra can reflect a shift to lower or higher wavenumber due to tensile and compressive stresses affected, as reported earlier. The characteristic transversal optical phonon (TO) mode (A1/E1) peak at 635 cm^{-1} of SnO_2 showed blue shift in general.

It is essential to mention that the peak associated with MnS grows as a function of the temperature of its precursor, and this result is supported by the orderly and consistent decrease of the peaks related to tin oxide, cadmium sulfide, and glass, which in the sample that exhibits larger deposit and higher quality have almost disappeared. Naturally, in this technique, minor peaks are seen that do not coincide with those of the materials mentioned above, possibly associated with another crystalline phase of MnS. Compressive stresses may have caused this shift in the CdS/MnS heterostructure, but we can observe a behavior in terms of intensity and thickness of the peaks similar to that of the characterization by X-ray diffraction analysis.

The observed Raman peaks are in agreement with the literature reports [5,23]. Aforementioned, the peak that interests us is of maximum length in the sample deposited at eighty degrees and the peaks of the materials below practically disappeared.

3.3. Optical characterization

Optoelectrical properties are obtained by UV–vis analysis, Figs. 5 and 6. MnS presents one absorption peak in the range of 354.28–480 nm. Surprisingly no significant differences were found in the UV–vis spectra of the CdS/MnS heterostructure for 60 °C and 80 °C, which was highly like the bare MnS spectrum. A possible explanation might be that MnS is more dominant in terms of both electron density and crystal size [22], causing a diminution in the absorption border for the CdS compound at 20C° and 40 °C highly

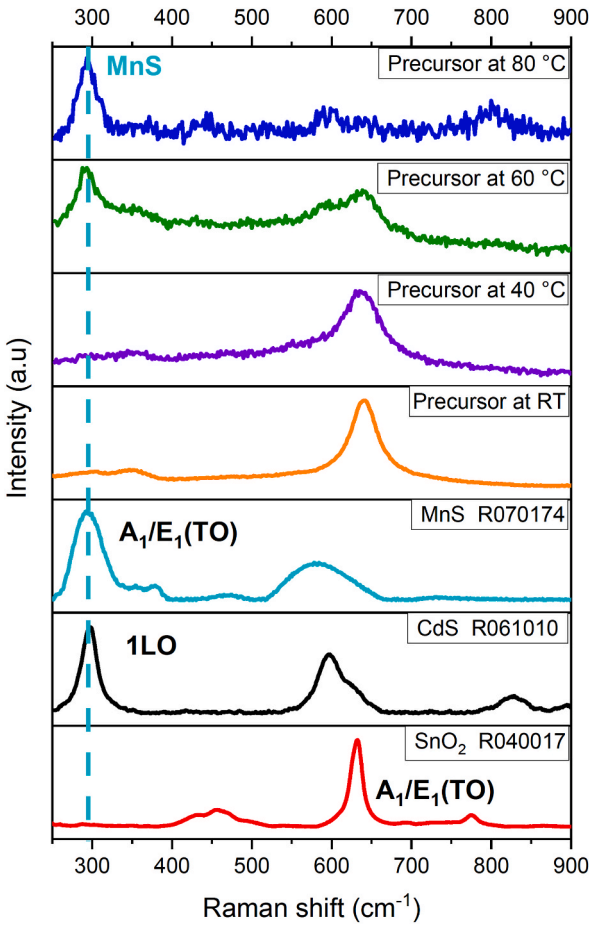

Fig. 4. MnS thin films Raman spectra. The diagram shows two principal peaks at ~300 and 645 cm^{-1}. The increase of the MnS peak is shows with a blue line, being directly proportional to the temperature of the precursor. (For interpretation of the references to colour in this figure legend, the reader is referred to the Web version of this article.)

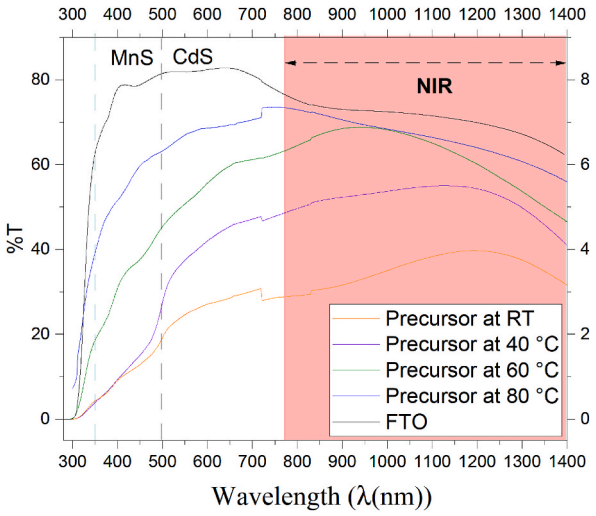

Fig. 5. Transmittance for the MnS thin films and the CdS/FTO substrate, the red zone in the figure shows the near-infrared (NIR) wavelength range and the dotted lines indicate the position where the peak associated with MnS and CdS, respectively, is found. (For interpretation of the references to colour in this figure legend, the reader is referred to the Web version of this article.)

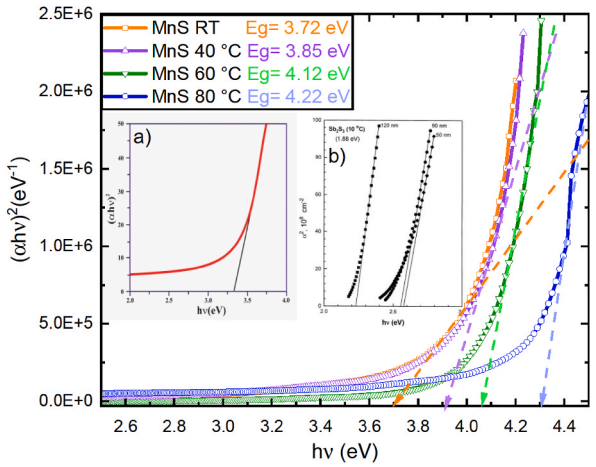

Fig. 6. Determination of bandgap for the MnS/CdS/FTO thin film deposited with a cationic precursor at room temperature, 40, 60 and 80 °C. Insets a) Tauc plot reference for the MnS thin film at 3.35 eV approximatively and b) Tauc plot reference for the CdS thin film at 2.5 eV approximatively.

related to the GIXRD effect. Fig. 5 exhibits spectrophotometric transmittance of a α-MnS film on FTO/CdS glass substrate. Can be seen that the deposited compounds are highly transparent with a 63% maximum value of transmittance (Fig. 4). A sharp ultraviolet cut-off was observed at approximately 285 nm and is attributed to the FTO substrate, for the film a slight deviation from the result present by Gümüs et al. [24]. A notorious behavior for all thin films deposited was observed in the range of 800–1400 nm, where the optical transmittance decreased to a minimum value transmittance (Fig. 5). This effect could explain a reflective response in the near-infrared spectra (NIR), which range in the wavelength corresponding to thermal energy, an effect that could be attributed to possible use as a low-e material [25]. The thickness of the thin films (d) was measured using a contact profilometer and transversal SEM (Fig. 8), the results were used to determinate the band gap of the materials. The band gap of the MnS thin film was determined by plotting $(\alpha h\nu)^2$ versus $(h\nu)$. The absorption coefficient for the allowed direct transition can be determined with a photon energy using the Stern's relation shown in equation (3) and the thickness of the films [11]:

$$\alpha = \frac{A}{h\nu}\left(h\nu - E_g\right)^{\frac{1}{2}} \tag{5}$$

The bandgap value for the thin film was determined at a range of 3.92–4.22 eV for the different thin films and depending of the variation in precursor temperature transmittance (Fig. 6).

We can observe a slight effect of the substrate in the transmission spectra, this effect causing a blue shift for the gap of the MnS thin

film as the thickness decreased (Fig. 7). Yildirim et al. show a similar bandgap value for the MnS thin film [8] according to Hannachi et al. [26] such value can be attribute to the $\alpha-$ MnS.

3.4. SEM

SEM images shown in Fig. 7 determine the surface properties of the films and directly influence their optical and electrical properties; it is notable from the SEM micrographs that at room temperature and 204. 2 nm of thick film does have a smooth and homogeneous surface morphology with a low presence of holes and cracks.

The dense, smooth and well-adherent to the substrate of the films decreases with decreasing film thickness (Fig. 8). Consequently, the surface properties of the MnS films appear to have changed significantly with the variation of the temperature in the cationic precursor. All surface properties, such as the number of cracks, lack, and material accumulation, decrease as temperature increases, especially for the 80 °C temperature and 124.6 $\pm$ 18.0 nm thickness. These results are in agreement with GIXRD measurements.

The frontal scanning electron microscopy (Fig. 8) shows an improvement in the uniformity as a function of the manganese chloride temperature. The transversal view (Fig. 7) was used to obtain the thicknesses of the incorporated material, from which, together with the uv–vis's characterization, the bandgap of the manganese can be determined (Fig. 6).

3.5. I–V curve

MnS thin films have several polycrystalline forms, the cubic modification has the rock-salt type structure (α-MnS) is the most common at RT [27], by low-temperature thin films grow into the wurtzite-type structure (γ- MnS) or zinc-blende-type (β-MnS) [17]. We have succeeded to prepare a polycrystalline α-MnS thin film at an 80 °C temperature by SILAR and suitable deposition conditions deposited in FTO/CdS compounds. Fig. 6 shows the final product of the process, for the diode we use the superstrate form that allows the device to be illuminated from the FTO glass substrate.

Fig. 9 shows the current-voltage (I–V) characteristic of the deposited film (Keithley 4200A-SCS parameter Analyzer). The elaborated layers at 20 °C, 40 °C y 60 °C presents a diode behavior. These diodes measured under illumination at 1000 W/m^2 did not present generation of voltage and current. The only diode that generated voltage was a 80 °C precursor sample. According to the data, Voc of 300 mV and JSC of 1.2μA/cm2 (Fig. 8) were determinate for MnS 80 °C sample. Fadaam et al. shows similar results for the MnS thin-film describing that the annealing process due to the control in the grain barrier and could increase the Voc [28].

Obvious cross-over behavior in the I–V curves is observed, which is believed to arise from illumination dependent electron barrier at the interface between the absorber and the buffer layer [29]. Additionally, the I–V curve shows a diode-marked behavior, this denotes a depletion zone or what is the same, knowing that the cadmium sulfide commonly has an n-type behavior, then the manganese sulfide is contributing with holes.

4. Conclusions

MnS thin films were synthesized on glass and CdS/FTO substrates using the SILAR method with equipment fabricated in the Universidad Autónoma de Zacatecas. The deposition was performed with different temperatures in the cationic precursor, showing a clearance variation in the qualities of the films, this from GIXRD and Raman, thus varying the lattice constant and the gap of the material, showing that at a higher temperature (80 °C) the better properties of the samples, even with a wide gap. However, the material can be used as a window layer in a photovoltaic device. The characteristic curve of the diode shows the existence of the

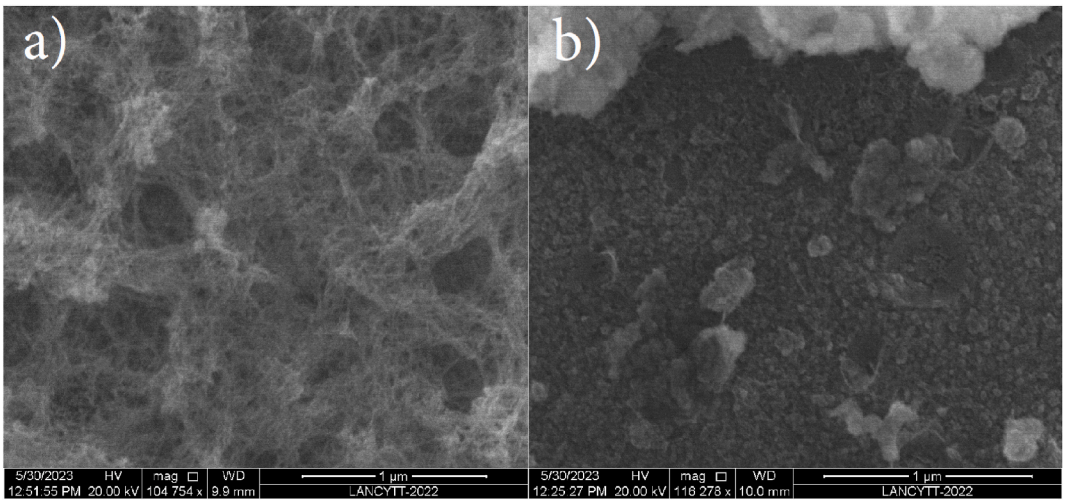

Fig. 7. SEM images for the MnS thin films synthetized at a) Room temperature and b) 80 °C.

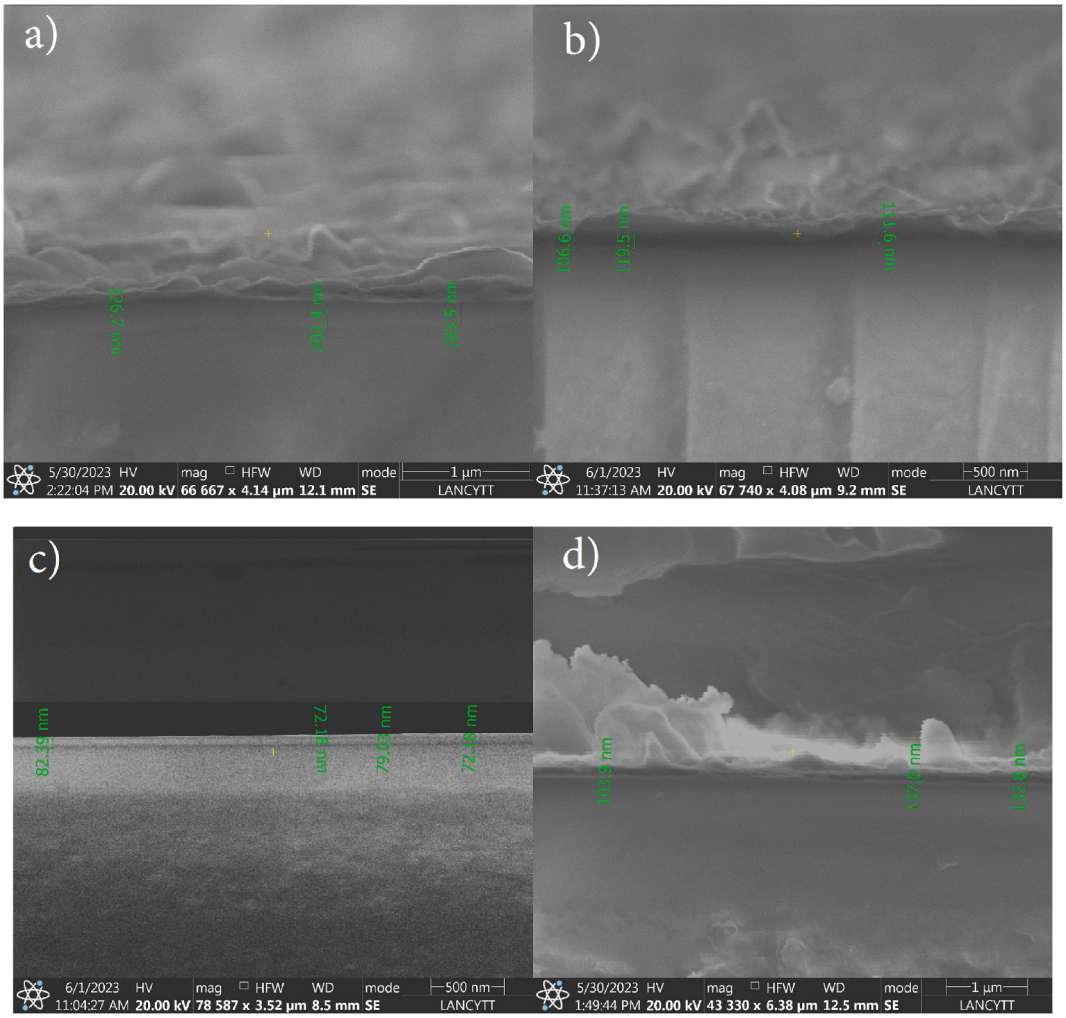

Fig. 8. Transversal view SEM images for the MnS thin films synthetized at a) Room temperature, b) 40, c) 60 and d) 80 °C respectively used to determined thickness for the samples.

expected charge carriers for these materials. The I–V characterization showed that MnS contributes with positive carrier for the manganese sulfide to the device to create a depletion region because, in these conditions, CdS is an n-type material. The X-rays and Raman spectroscopy characterization support having MnS in its cubic phase in all cases with physical and chemical properties similar to those reported in other articles, validating a success in the material synthesis. We determine that our deposit is of the -MnS type and the p-type since the characteristic I–V curve of a diode is presented, and the sample with 80°c precursor produces the best values of V_{oc} and ISC of our samples. Electrical characterization shows values appropriate for an electronic device or an absorber layer for a solar cell as an optical value due to its wide bandgap. The XRD determined the capacities of the method to deposit semiconductors with an acceptable crystallinity. In conclusion, the variation in the temperature of the precursor affects the physical properties, indicating 80 °C as the choice of process temperature for the synthesis of α-MnS by the SILAR method.

CRediT authorship contribution statement

H. Moreno-García: Writing – review & editing, Project administration. **J.O. Sigala-Valdez:** Writing – review & editing, Writing – original draft, Investigation, Formal analysis, Data curation. **Ma del Rosario Martínez-Blanco:** Project administration, Conceptualization. **I. Cruz Reyes:** Validation, Software, Resources, Formal analysis. **S.M. Durón-Torres:** Writing – review & editing, Software. **I.L. Escalante-García:** Writing – review & editing, Validation, Project administration, Formal analysis. **A. Del Rio-De Santiago:** Writing – review & editing, Writing – original draft, Validation, Supervision, Software, Resources, Funding acquisition, Formal analysis, Conceptualization.

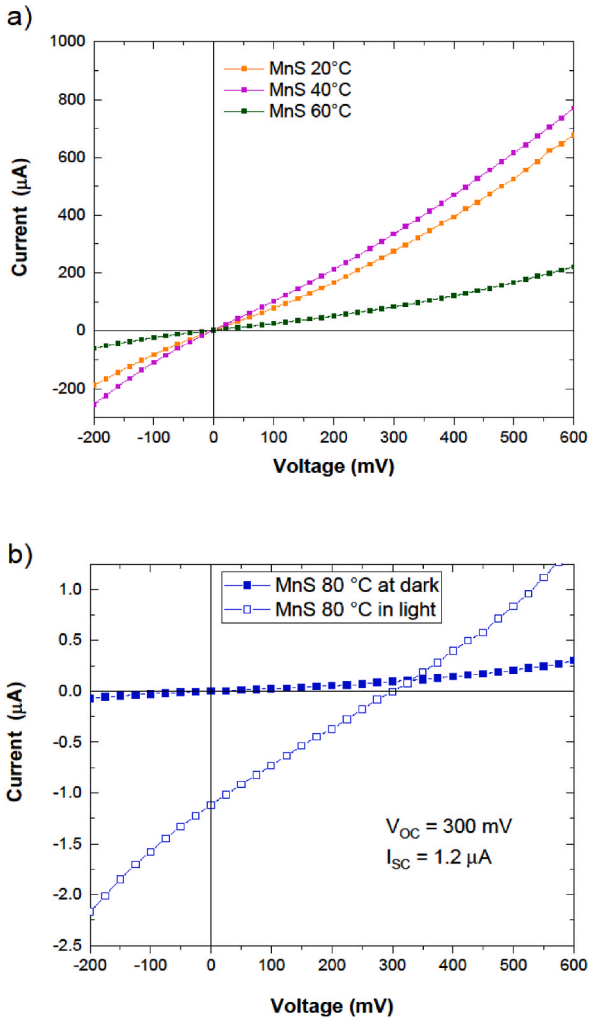

Fig. 9. I–V curve to the samples FTO/CdS/MnS/graphite a) in darkness for the diodes elaborated with samples MnS 20 °C, MnS 40 °C and MnS 60 °C. The I–V curve in b) correspondent to diode with MnS 80 °C, measured in darkness (solid symbol) and illumination (open symbols). The VOC is 300 mV and the current density is 1.2 μA/cm2 for sample MnS 80 °C.

Declaration of competing interest

The authors declare that they have no known competing financial interests or personal relationships that could have appeared to influence the work reported in this paper.

Acknowledgments

The authors extend their thanks: Convocatoria para Adquisición y Mantenimiento de Infraestructura en Instituciones y Laboratorios de investigación Especializada 2019, Proyecto: 299812 Proyecto infraestructura complementaria para la caracterización de películas delgadas semiconductoras. Responsable técnico Harumi Moreno Garcia, for the technical support they provided.

The authors extend their thanks: “Laboratorio nacional de análisis físicos, químicos y biológicos”

References

[1] A.Y. Cho, J.R. Arthur, Molecular beam epitaxy, Prog. Solid State Chem. 10 (Jan. 1975) 157–191, https://doi.org/10.1016/0079-6786(75)90005-9.

[2] H. Zhang, et al., A CdS/MnS p–n heterojunction with a directional carrier diffusion path for efficient photocatalytic H_2 production, Inorg. Chem. Front. 9 (6) (2022) 1100–1106, https://doi.org/10.1039/D1QI01632F.

[3] P. Sigmund, Theory of Sputtering. I. Sputtering yield of amorphous and polycrystalline targets, Phys. Rev. 184 (2) (Aug. 1969) 383–416, https://doi.org/10.1103/PhysRev.184.383.

[4] T. Dhandayuthapani, R. Sivakumar, C. Sanjeeviraja, C. Gopalakrishnan, S. Arumugam, Microstructure, optical and magnetic properties of micro-crystalline γ-MnS film prepared by chemical bath deposition method, Mater. Sci. Semicond. Process. 72 (Dec. 2017) 67–71, https://doi.org/10.1016/j.mssp.2017.09.025.

[5] X. Jin, et al., Manganese sulfate-derived α/γ-MnS embedded in N-doped layered carbon for high-performance lithium-ion batteries, Mater. Today Chem. 24 (Jun. 2022) 100992, https://doi.org/10.1016/j.mtchem.2022.100992.
[6] M.A. Yıldırım, S.T. Yıldırım, İ. Cavanmirza, A. Ateş, Chemically synthesis and characterization of MnS thin films by SILAR method, Chem. Phys. Lett. 647 (Mar. 2016) 73–78, https://doi.org/10.1016/j.cplett.2016.01.048.
[7] A. Del Río-De Santiago, J.C. Martínez-Orozco, K.A. Rodríguez-Magdaleno, D.A. Contreras-Solorio, I. Rodríguez-Vargas, F. Ungan, Intermediate band formation in a δ -doped like QW superlattices of GaAs/Al x Ga 1−x as for solar cell design, Superlattice. Microst. 115 (Mar. 2018) 191–196, https://doi.org/10.1016/j.spmi.2018.01.029.
[8] H. Ohno, Bridging semiconductor and magnetism, J. Appl. Phys. 113 (13) (Apr. 2013) 136509, https://doi.org/10.1063/1.4795537.
[9] G.A. Tigwere, et al., Molecular precursor route for the phase selective synthesis of α-MnS or metastable γ-MnS nanomaterials for magnetic studies and deposition of thin films by AACVD, Mater. Sci. Semicond. Process. 139 (Mar. 2022) 106330, https://doi.org/10.1016/J.MSSP.2021.106330.
[10] A. Del Río-De Santiago, et al., Nanostructure formation during relatively high temperature growth of Mn-doped GaAs by molecular beam epitaxy, Appl. Surf. Sci. 333 (Apr. 2015) 92–95, https://doi.org/10.1016/j.apsusc.2015.01.228.
[11] C.D. Lokhande, et al., Process and characterisation of chemical bath deposited manganese sulphide (MnS) thin films, Thin Solid Films 330 (2) (Sep. 1998) 70–75, https://doi.org/10.1016/S0040-6090(98)00500-8.
[12] M. Ristov, Gj Sinadinovski, I. Grozdanov, Chemical deposition of Cu2O thin films, Thin Solid Films 123 (1) (Jan. 1985) 63–67, https://doi.org/10.1016/0040-6090(85)90041-0.
[13] Y.F. Nicolau, SOLUTION DEPOSITION OF THIN SOLID COMPOUND FILMS BY A SUCCESSIVE IONIC-LAYER ADSORPTION AND REACTION PROCESS *, 1985.
[14] S.J.A. Zaidi, S. Zoha, M. Ahmad, M. Shahid, T.J. Park, M.A. Basit, Physicochemically tailored Ag2S QDs deposition on ZnO for improved photocatalytic and antibacterial performance, Mater. Today Commun. 37 (Dec. 2023), https://doi.org/10.1016/j.mtcomm.2023.107016.
[15] A. Azhar, et al., Synchronized wet-chemical development of 2-dimensional MoS2 and g-C3N4/MoS2 QDs nanocomposite as efficient photocatalysts for detoxification of aqueous dye solutions, Colloids Surf. A Physicochem. Eng. Asp. 657 (Jan. 2023), https://doi.org/10.1016/j.colsurfa.2022.130581.
[16] U.J. Awan, M.A. Basit, S.I.A. Shah, J. Yong-Xin, H. Zhifu, Minimized OER overpotential via SILAR-based development of g-C3N4/CdS nanocomposite, Appl. Phys. A 129 (12) (Dec. 2023) 850, https://doi.org/10.1007/s00339-023-07105-y.
[17] C. Ulutas, M. Gunes, C. Gumus, Influence of post-deposition annealing on the structural and optical properties of γ -MnS thin film, Optik 164 (Jul. 2018) 78–83, https://doi.org/10.1016/j.ijleo.2018.02.118.
[18] P.K. Nair, et al., Semiconductor Thin Films by Chemical Bath Deposition for Solar Energy Related Applications, 1998.
[19] Charles Kittel, Introduction to Solid State Physics, eighth ed., John Wiley & Sons, New York, NY, 2024.
[20] A.R. Stokes, A.J.C. Wilson, The diffraction of X rays by distorted crystal aggregates - I, Proc. Phys. Soc. 56 (3) (May 1944) 174–181, https://doi.org/10.1088/0959-5309/56/3/303.
[21] M.A. Yıldırım, S.T. Yıldırım, İ. Cavanmirza, A. Ateş, Chemically synthesis and characterization of MnS thin films by SILAR method, Chem. Phys. Lett. 647 (Mar. 2016) 73–78, https://doi.org/10.1016/j.cplett.2016.01.048.
[22] A.İ. Vaizoğullar, An effective photocatalytic and photoelectrochemical performance of β/γ-MnS/CdS composite photocatalyst for degradation of flumequine and oxytetracycline antibiotics under visible light irradiation, J. Mater. Sci. 55 (9) (Mar. 2020) 4005–4016, https://doi.org/10.1007/s10853-019-04299-6.
[23] T. Dhandayuthapani, R. Sivakumar, C. Sanjeeviraja, C. Gopalakrishnan, S. Arumugam, Microstructure, optical and magnetic properties of micro-crystalline γ -MnS film prepared by chemical bath deposition method, Mater. Sci. Semicond. Process. 72 (Dec. 2017) 67–71, https://doi.org/10.1016/j.mssp.2017.09.025.
[24] C. Gümüş, C. Ulutaş, Y. Ufuktepe, Optical and structural properties of manganese sulfide thin films, Opt. Mater. 29 (9) (May 2007) 1183–1187, https://doi.org/10.1016/j.optmat.2006.04.012.
[25] Z. Montiel-González, O.Y. Ramírez-Esquivel, D. Cabrera-German, J.A. Torres-Ochoa, A.A. Ortíz-Atondo, D.A. Mazón-Montijo, Structural, chemical, and MIR response of covellite CuS films via SILAR as opaque Low-E coatings, Opt. Mater. 126 (Apr. 2022) 112208, https://doi.org/10.1016/j.optmat.2022.112208.
[26] A. Hannachi, S. Hammami, N. Raouafi, H. Maghraoui-Meherzi, Preparation of manganese sulfide (MnS) thin films by chemical bath deposition: application of the experimental design methodology, J. Alloys Compd. 663 (Apr. 2016) 507–515, https://doi.org/10.1016/j.jallcom.2015.11.058.
[27] T. Ganguli, A. Ingale, Raman and photoluminescence investigations of disorder in ZnSe films deposited on *n* -GaAs, Phys. Rev. B 60 (16) (Oct. 1999) 11618–11623, https://doi.org/10.1103/PhysRevB.60.11618.
[28] S.A. Fadaam, H.M. Ali, A.H. Shaban, S.A. Ahmed, Improving Efficiency of Solar Cell for MnS through Annealing, 2020 020030, https://doi.org/10.1063/5.0033260.
[29] X.D. Gao, X.M. Li, W.D. Yu, Morphology and optical properties of amorphous ZnS films deposited by ultrasonic-assisted successive ionic layer adsorption and reaction method, Thin Solid Films 468 (1–2) (Dec. 2004) 43–47, https://doi.org/10.1016/j.tsf.2004.04.005.